International Journal of Mechanical, Industrial and Aerospace Sciences
ISSN: 2517-9950
Vol:14, No:3, 2020

# Simplified Stress Gradient Method for Stress-Intensity Factor Determination

Jeries J. Abou-Hanna

***Abstract*—**Several techniques exist for determining stress-intensity factors in linear elastic fracture mechanics analysis. These techniques are based on analytical, numerical, and empirical approaches that have been well documented in literature and engineering handbooks. However, not all techniques share the same merit. In addition to overly-conservative results, the numerical methods that require extensive computational effort, and those requiring copious user parameters hinder practicing engineers from efficiently evaluating stress-intensity factors. This paper investigates the prospects of reducing the complexity and required variables to determine stress-intensity factors through the utilization of the stress gradient and a weighting function. The heart of this work resides in the understanding that fracture emanating from stress concentration locations cannot be explained by a single maximum stress value approach, but requires use of a critical volume in which the crack exists. In order to understand the effectiveness of this technique, this study investigated components of different notch geometry and varying levels of stress gradients. Two forms of weighting functions were employed to determine stress-intensity factors and results were compared to analytical exact methods. The results indicated that the "exponential" weighting function was superior to the "absolute" weighting function. An error band +/- 10% was met for cases ranging from a steep stress gradient in a sharp v-notch to the less severe stress transitions of a large circular notch. The incorporation of the proposed method has shown to be a worthwhile consideration.

***Keywords*—**Fracture mechanics, finite element method, stress intensity factor, stress gradient.

## I. Introduction

FRACTURE mechanics has been called one of the most important developments in the entire field of mechanics. Using the stress-intensity factor assists in describing the elastic stress field in the vicinity of cracks. Not all techniques for determining stress-intensity factors share the same merit. In addition to overly-conservative results, methods that are computationally intensive, situation specific, and those requiring copious user parameters hinder a practicing engineer from efficiently generating practical stress-intensity factors. The intent of this work was to investigate if a stress-gradient based reduced-complexity method for determining stress-intensity factors can both significantly enhance user friendliness and attain levels of accuracy similar to complex conventional methods. It is assumed that in order for the failure process to occur it requires a physical volume, containing some flaw size, to be subjected to an effective stress [1]-[4].

Jeries J. Abou-Hanna is with the Bradley University, United States (e-mail: jannah@bradley.edu).

## II. Literature Background

A traditional approach is built from the following foundational equation used by Irwin [5], to describe stress intensity under elastic stress field in the vicinity of a crack tip:

$$K = F\sigma\sqrt{\pi a} \tag{1}$$

where "$F$" is used to represent all necessary correction factors indicated in the various works by investigators such as Murakami [6].

Additional modifications to (1) involve substitution of the crack-length term "$a$" with variables representing a notch-tip radius [7], or a notch depth. Works by Murakami [8]-[11] indicated that the stress-intensity factor can be determined as a function of $\sqrt{area}$, within an accuracy of 10% in the linear-elastic fracture mechanics range. A limitation of this method resides in the use of a single "applied stress" that may not be readily available or present in engineering components or under complex multi-axial stress conditions. The analysis of stress-intensity factors has also been considered using the body force method [12], [13]. Perez et al. [14] and Liu and Mandevan [15] employed numerical interpolation while capitalizing on existing solutions and expressions to calculate stress-intensity factors. Chell [16], [17] indicated that the stress-intensity factor for an arbitrary loaded crack could be written as the product of the compliance function for the given crack subjected to a uniform stress and a weighted integral involving the arbitrary stress. Further methods incorporating the use of stresses across the length of the crack or flaw are seen in the ASME Code [18] and in [19]. Bueckner [20] and Rice [21] developed the weight function method, to calculate stress-intensity factors. Several researchers have utilized the FEA methods or variants of them to determine stress-intensity factors. Liu et al. [22], Ju and Chung [23], and Xu et al. [24] employed the stresses obtained from FEA to calculate stress-intensity factors. The ability to evaluate stress-intensity factors for non-standard crack configurations is a significant attraction for the use of FEA. However, the high stress gradients near a crack tip require very refined meshes and special elements, resulting in an arduous task to model a crack.

Works by Taylor and others [25], [26] use volumetric average stress around the crack and utilize critical distance approach which requires experimental data. Cost and 10% uncertainty in results work against this method.

## III. Proposed Method

### *A. Stress-Intensity Factor Determination Using Stress Gradients*

The method begins with a crack free a linear-elastic FEA on the modeled component. The maximum principal stress was chosen for consideration throughout this work. A "local maximum stress point" that exists on the component surface (known as the local maximum surface stress point or LMSSP) is identified. Focus is on Mode I stress-intensity factor. The LMSSP is used as the origin for a radial-distance layering process applied to the surrounding stress field. Moving inward from the component surface, the internal volume is divided into multiple spherical layers (for a 3D model) or radial layers (for a 2D model) that surround the LMSSP. A 2D representation of the layering method is shown in Fig. 1. The stress values contained within each individual layer are then simply averaged. This averaging operation results in a 1D curve of stress vs. distance from component surface, Fig. 2. Using the 1D stress profile and an appropriate curve-smoothing procedure enables a determination of the local stress gradient defined as:

$$\bar{\chi} = \frac{\partial \sigma(x)}{\partial x}, \tag{2}$$

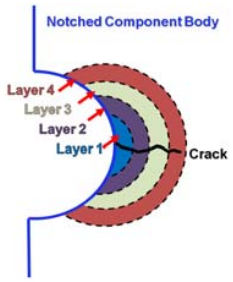


Fig. 1 Radial Layering Method

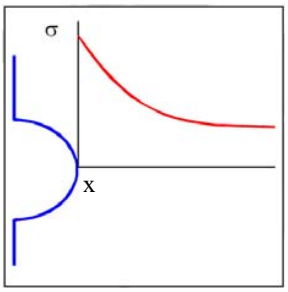


Fig. 2 1D Averaged Stress Curve

The proposed method accounts for the stress gradient effect through the use of a distance-based weighting scheme and the relative stress gradient. The local stress gradient is utilized in the relative stress gradient, defined according to:

$$\chi(x) = \frac{1}{\sigma(x)} \frac{\partial \sigma(x)}{\partial x} = \frac{1}{\sigma(x)} \bar{\chi}. \tag{3}$$

The weighting function, $\phi(x,\chi)$, utilizes the relative stress gradient along with the distance from the LMSSP to modify the stress profile through the following operation:

$$\sigma_W(x) = \sigma_{1D}(x)\phi(x,\chi) \tag{4}$$

where $\sigma_W$ is the resulting weighted stress profile, $\sigma_{1D}$ is the 1D stress profile from the averaged layers, and $\phi(x,\chi)$ is the weighting function (described later). The weighted 1D stress ($\sigma_W(x)$) profile is averaged together to arrive at a single effective stress for the physical volume/area considered for the stress-intensity factor calculation. Determination of exactly how much of the stress profile to average is guided by [1], [2] by considering that a critical volume of material exists, influenced by both the effective stress and effective distance, and is established through use of the relative stress gradient. Therefore, the distance from the LMSSP to the minimum point of the relative stress gradient, defined as "$x_{eff}$", corresponds to the range of the stress profile which should be averaged. Fig. 3 illustrates an example of a relative stress gradient with a minimum point at 1.2, thereby establishing that the weighted stress profile should be averaged from $x$ = 0 (LMSSP) to $x$ = 1.2 ($x_{eff}$ =1.2) in the determination of the effective stress.

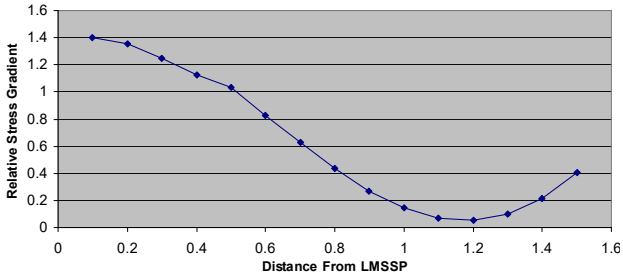


Fig. 3 Minimum Relative Stress Gradient at 1.2

Subsequently, using the $x_{eff}$ distance from the relative stress gradient, a calculation of the equivalent stress value would follow:

$$\sigma_{eq} = \frac{1}{x_{eff}} \int_{x=0}^{x_{eff}} \sigma_W dx. \tag{5}$$

The equivalent stress value will be incorporated into a "standard" stress-intensity with proposed final form of the stress-intensity factor:

$$K = \sigma_{eq,a} \sqrt{\pi a} \tag{6}$$

where "$a$" represents the crack size which can range up to the maximum length of $x_{eff}$.

## IV. Investigation of the Proposed Method

The investigation of the proposed method was accomplished through the comparison of the method-derived

stress-intensity factors to those readily available in engineering handbooks. Cases, described later, were chosen to accentuate various degrees of possible gradients.

## V. Assumptions

It is important to ensure that the crack dimensions would be small against the size of the component for LEFM conditions to prevail. Also state of plane strain was assumed.

## VI. Case Studies

### *A. A Crack Emanating from a Round Hole in a Plate Under Uniaxial Tension*

The approach is explained through this first case. Multiple hole diameters were investigated ranging from 1-250 mm. A quarter symmetry mesh model is shown in Fig. 4. A 100 MPa uniform pressure was applied across the top edge. The material properties represent alloy steel with a modulus of elasticity of 205 GPa and a Poisson's ratio of 0.29. The LMSSP corresponded to the left-most element along the line of horizontal symmetry, shown in Fig. 5.

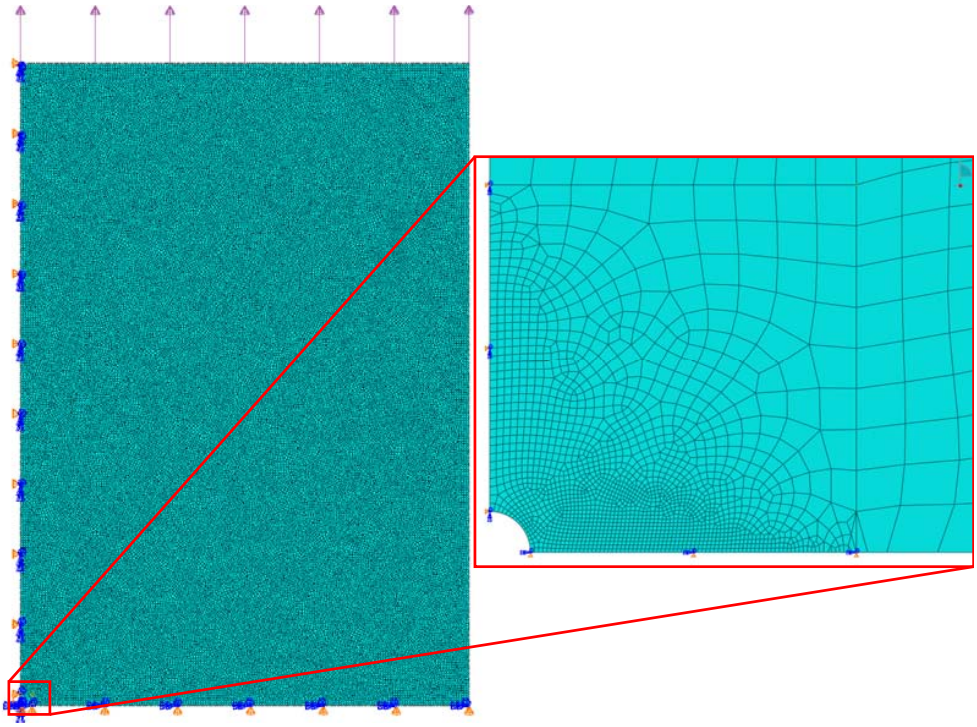

Fig. 4 Quarter Symmetry Model for 1-mm Hole Case

Fig. 6 shows the stress radial layers; the black vertical line shows the surface boundary. The arrow points to the region of elements used for stress analysis. The stress values for each layer were subsequently averaged. Then the resulting single-layer stress value was modified through the weighting process, as described later. The following example (2-mm diameter hole) will represent how each case was handled.

A minimum of ten radial layers should be established as an initial starting point for the analysis. Additionally, with the limit to the usable defect size corresponding to the distance from the LMSSP to the minimum point of the relative stress gradient, at least 50% of these initial layers should exist within this limiting distance. The necessity of having layers beyond the minimum point of the relative stress gradient is a direct consequence of not knowing *a priori* where the minimum weighted stress point will be located within the stress field. The stress results from the 2 mm case were processed using two different weighting functions. Choice of weight functions was influenced by [27], [28], which indicated the advantages of using volumetric weight functions that deliver instantaneous response in terms of relative stress gradients and distance from a notch root. Following the layer averaging, a fourth-order polynomial was fitted to the stress values. The polynomial fitting was used to reduce extreme fluctuations in the stress derivatives ($\Delta\sigma/\Delta x$) as seen in Fig. 7.

The stress gradient was then determined by taking a derivative with respect to distance. Further, an absolute stress gradient was determined for each layer's distance from the LMSSP using the following equation:

$$\bar{\chi}_{absi} = \bar{\chi} x_i, \tag{7}$$

where $x_i$ corresponds to each layer's distance from the LMSSP. The absolute stress gradient values were divided by each corresponding layer's average stress value (shown in (7)) to arrive at the relative stress gradient results in Fig. 8.

$$\chi_i = \frac{\bar{\chi}_{absi}}{\sigma_i} \quad (8)$$

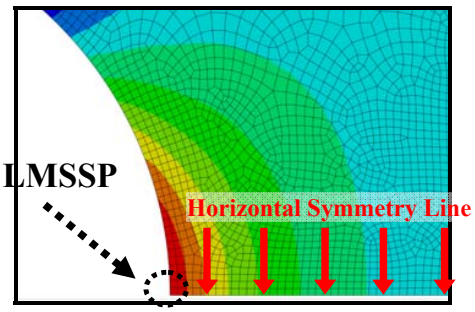


Fig. 5 LMSSP for Flat Plate with Circular Hole

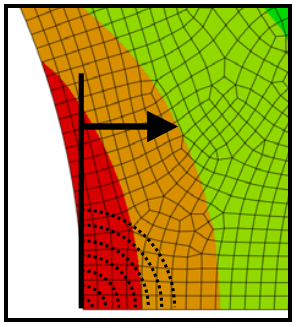

Fig. 6 Radial Layer Construction on a Quad-Dominated Mesh Technique

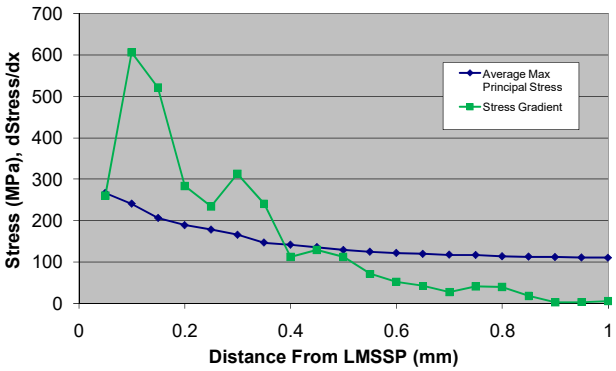


Fig. 7 Stress Gradient Fluctuations Resulting from dσ/dx Operation on Average Stress Values.

Fig. 8 shows the minimum point of the relative stress gradient, $x_{eff}$, at a distance of 1.2 mm from the LMSSP. This distance to the averaged 1D stress-field inflection point establishes the limit to how much of the stress profile can be utilized in calculations for the stress-intensity factor.

Prior to completing the stress-intensity factor calculation, the stress values for each layer are processed through a weighting function. As indicated, two weighting functions, "absolute" and "exponential", were utilized in the investigation. They are a function of the relative stress gradient and the distance of the layer from the LMSSP. The absolute weighting function is defined as:

$$Absolute(\chi, x) = 1 - |\chi_i| x_i \quad (8)$$

while the exponential weight function is denoted as:

$$Exponential(\chi, x) = e^{\chi_i x_i / 2} \quad (9)$$

The weight functions for each layer are shown in Fig. 9.

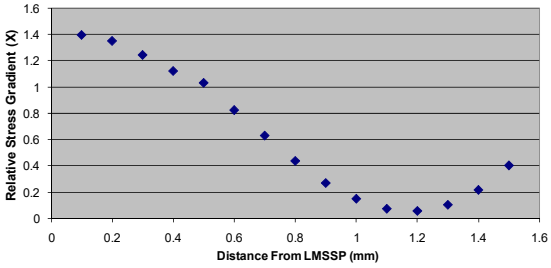


Fig. 8 Relative Stress Gradient for 2 mm Case

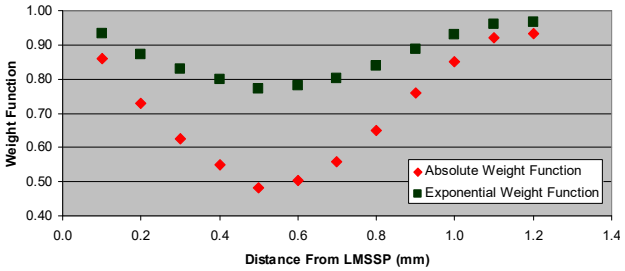


Fig. 9 Weight Function Comparison for 2 mm Case

The product of the weight function and stress values for each layer were calculated as displayed in Fig. 10. The weighted stresses are then utilized in determining stress-intensity factors for different defect sizes. This process is completed by using the defect length "*a*" to average all the stress layers that are contained within this length and produce an average equivalent stress value, $\sigma_{eq,a,}$ , and it is incorporated into a standard stress-intensity factor equation as follows:

$$K = \sigma_{eq,a} \sqrt{\pi a} \,. \quad (10)$$

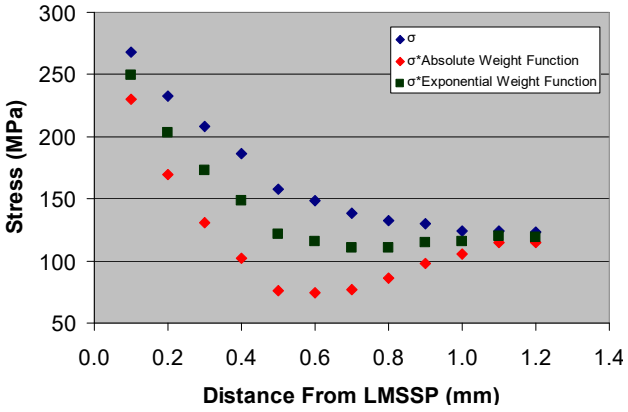


Fig. 10 Baseline and Weighted Stress Values (2 mm Case)

TABLE I
DEFECT SIZE, HANDBOOK, ABSOLUTE, AND EXPONENTIAL STRESS-INTENSITY FACTORS (MPA*M$^{0.5}$).

| Defect Size (m) | $\sigma_{eq}$ Absolute (MPa) | K Absolute | K Tada | K Absolute % Error |
|---|---|---|---|---|
| 0.0005 | 141.93 | 5.63 | 7.23 | -22.20 |
| 0.001 | 115.18 | 6.46 | 8.09 | -20.20 |
| 0.0012 | 114.20 | 7.30 | 8.42 | -16.08 |
| Defect Size (m) | $\sigma_{eq}$ Exponential (MPa) | K Exponential | K Tada | K Exponential % Error |
| 0.0005 | 179.35 | 7.11 | 7.23 | -1.69 |
| 0.001 | 146.44 | 8.21 | 8.09 | 1.46 |
| 0.0012 | 139.58 | 8.92 | 8.42 | 3.47 |

For example, if the defect size is 0.6 mm, the stress values of the layers within this distance would be utilized in (4) to produce the corresponding equivalent stress and stress-intensity factor. Following this logic, stress-intensity factors for various defect sizes, up to the permissible limit of 1.2 mm-- Xeff, were computed (Table I), and compared to handbook solutions given by Tada et al [29]. This process was used for several notch sizes, with errors shown in Figs. 11 and 12.

Errors using the "absolute" weight function range from -22.2 to 12.3%, while the "exponential" weighting function produced an error range of -9.5 to 13.74%.

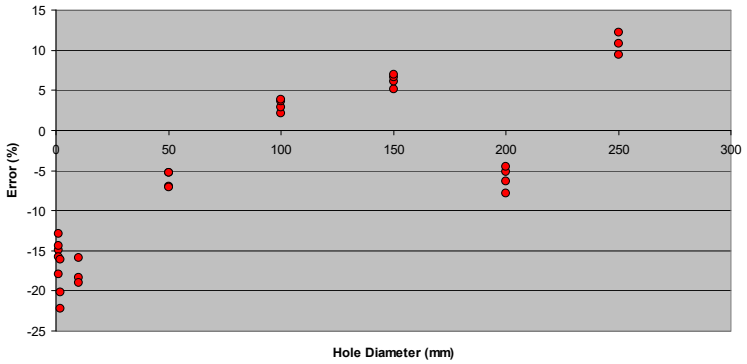


Fig. 11 Error in Stress-Intensity Factor Using Absolute Weighting Function

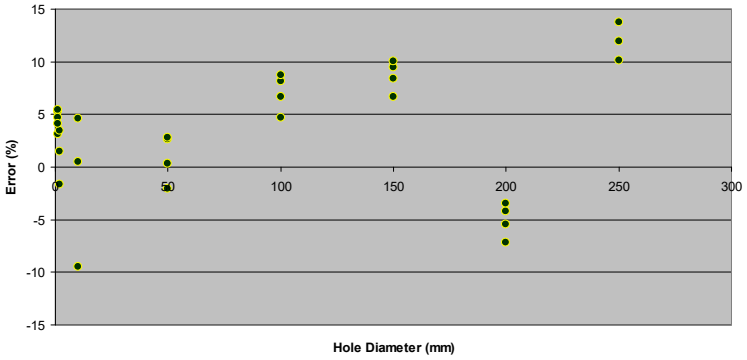


Fig. 12 Error in Stress-Intensity Factor Using Exponential Weighting Function

*B. A v-Notched Cracked Plate under Pure Tension*

Two notch angles were investigated, and they are 60 and 120 degrees, respectively. The half-symmetry model is shown in Fig. 13, with a close-up of the notch. A 100 MPa uniform pressure is applied across the top edge. The vertical boundary and a representation of the radial layer construction are shown in Fig. 14. The stress intensity computation process described earlier is utilized. The resulting relative stress gradients are Fig. 15. The minimum point of the relative stress gradient, $x_{eff}$, occurs at a distance of 1.25 mm from the LMSSP. The secondary minimum point at approximately 2.5 mm is a byproduct of the fourth-order polynomial fitting. Fig. 16 shows the stress intensity results against handbook values [29]. Fig. 17 shows the 120-degree case results. Errors for the "absolute" function ranged from -44 to -32 and -34 to -20% for the 60 and 120-degree cases, respectively. Errors for the "exponential" function ranged from -7 to 8 and -2 to 14% for the 60 and 120-degree cases, respectively.

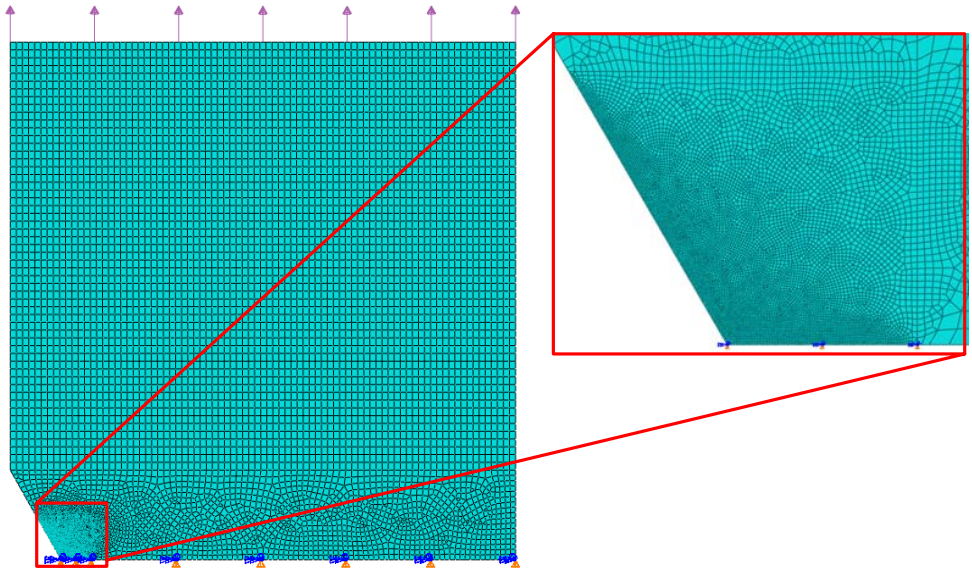

Fig. 13 Half-Symmetry Model for 120-Degree V-Notch Case

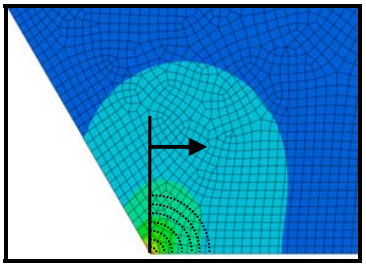

Fig. 14 Radial Layer Construction on a Quad-Dominated Mesh Technique

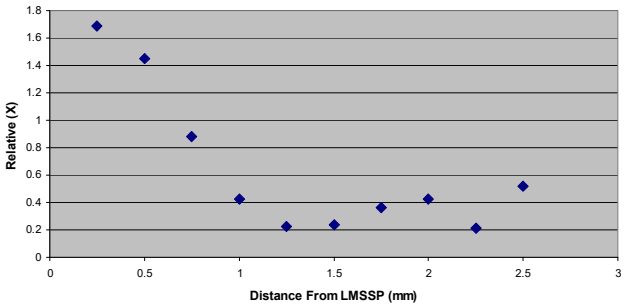


Fig. 15 Relative Stress Gradient for 60-Degree Case

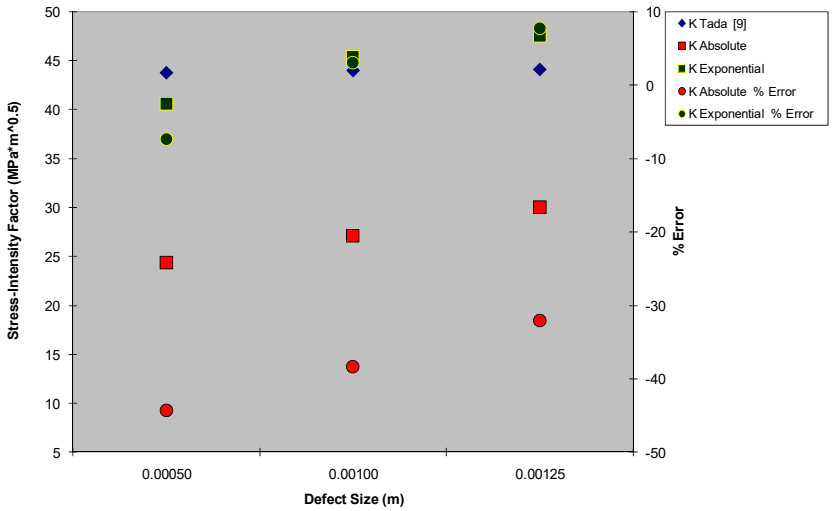


Fig. 16 Stress Intensity Factors and Error for 60-Degree V notch Case

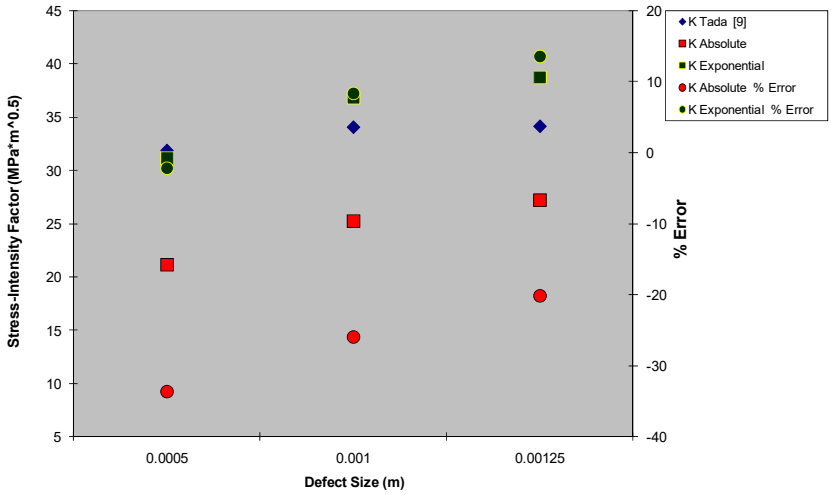


Fig. 17 Stress Intensity Factors and Error for 120-Degree V notch Case

### *C. A Pressurized Thick Cylinder with an Internal Crack*

The cylinder contains an internal circumferential crack spanning 360 degrees. A closed-form stress solution was used. Table II displays the different inside and outside radii (Ri, Ro) and thickness (t) used. Since relative stress gradient was linear, the minimum point corresponds to the outer wall radius. Three limiting distances were used for stress-intensity factor determination (1 mm, 5.3 mm, and 10.6 mm), using the established process described in case i, and the results are in Fig. 18. Using the "absolute" weighting function resulted in stress-intensity factor errors ranging from -54 to -4%, while using the "exponential" weighing function produced an error range of -53 to -2%. Also, using the smallest wall thickness (Configuration 3) produced the large error occurring at crack size of 0.005 m.

TABLE II
THICK CYLINDER CASE CONFIGURATIONS

| Configuration | 1 | 2 | 3 |
|---|---|---|---|
| Pi (MPa) | 6 | 6 | 6 |
| Ri (mm) | 32 | 20 | 13.33 |
| Ro(mm) | 64 | 40 | 20 |
| Ro/Ri | 2 | 2 | 1.5 |
| t (mm) | 32 | 20 | 6.67 |

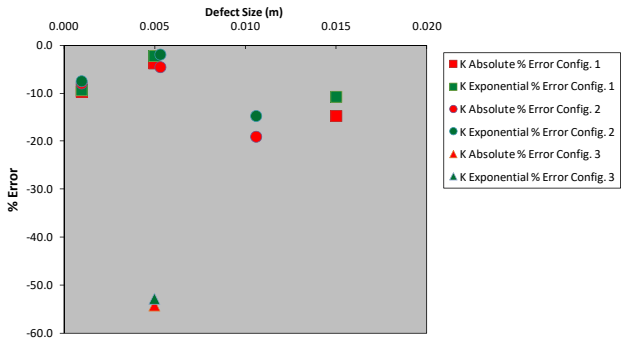


Fig. 18 Stress-Intensity Factor % Error for All Configurations-Thick Cylinder

## VII. OBSERVATIONS AND CONCLUSIONS

Two primary factors that indicate a divergence in the degree of accuracy are the weighting function and the shape of the stress profile. For cases where the proposed method produced stress-intensity factor results within +/- 10% of the handbook solution, more occurred utilizing the exponential weighting function as in Table III.

TABLE III
WEIGHT FUNCTION ACCURACY COMPARISON

| Case | Number of Results within +/- 10% of Textbook Solution | |
|---|---|---|
| | Absolute Weighting Function | Exponential Weighting Function |
| Cicular Notch | 13 | 28 |
| V-Notch | 0 | 3 |
| Cylinder | 4 | 5 |

With twice as many results falling within +/- 10% of the handbook solution, the exponential weighting function has a better performance. When considering the weighting value as a function of the relative stress gradient, one can see from Figs. 19-22 that the absolute weighting function generates more occurrences of lower numerical weighting. Figs. 20 and 22 focus on the highly populated lower relative stress gradients (for both weighting functions) that occur in cases with high stress gradients. The sensitivity of the absolute weighting function to steep gradients results in lower equivalent stress. With gentler stress gradients, the weighting values tend to stay within 0.9-1 and produce higher equivalent stress and more frequency of being in the +/- 10% error band. One can see from the error values that the exponential weight function is preferred.

For cases of linear or constant stress, the proposed method was unable to signify a permissible effective distance ($x_{eff}$) and generated inconsistent and sometimes large errors in stress-intensity factors. Although it was shown in the axi-symmetric pressure cylinder case that stress-intensity factor error could be within a +/- 10% range (-2.25% for Configuration 1, defect size 0.005 m) a change in the dimensions of the cylinder

resulted in a greater error for the same defect size (-53% for Configuration 3). But the extreme nature of the configuration should be investigated. In both cases, errors over 50% were generated from effective distances that equaled or exceeded half of the ligament length, which do not conform to LEFM criterion. When excluding the results of these two extreme configurations, the maximum error would be 20% (using the exponential weighting function).

The method is effective in generating values within 10% error band for a wide range of non-linear stress profiles with the exponential weighting function. Additionally, the modeling and solution time was fairly short. Adoption of the technique with a finite element software would likely necessitate automation scheme for computing stress averages in layers. Some errors were negative which indicates that the proposed method can be non-conservative. A possible solution is to include an additional factor into the calculation of the final stress-intensity factor. Revisiting the degree of negative error values suggests that a 1.2 multiplication factor can be considered sufficient to elevate the results in the conservative realm. However, this will likely result in increased and potentially unwanted levels of conservatism for some other cases. Therefore, as with other factors of safety an understanding of the potential ramifications from including a 1.2 multiplication factor cannot be understated.

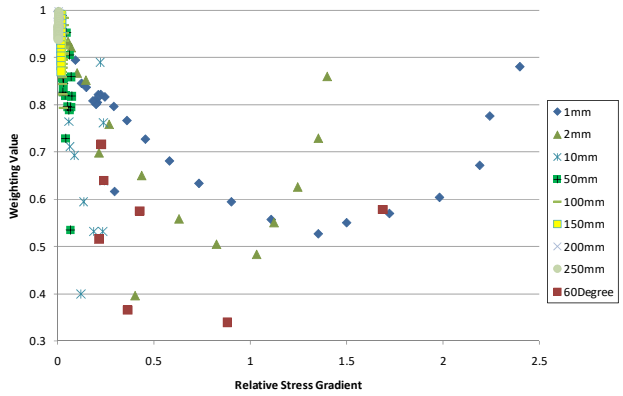


Fig. 19 Absolute Weighting Function Values for Notch Cases (0-2.5 Relative Stress Gradient)

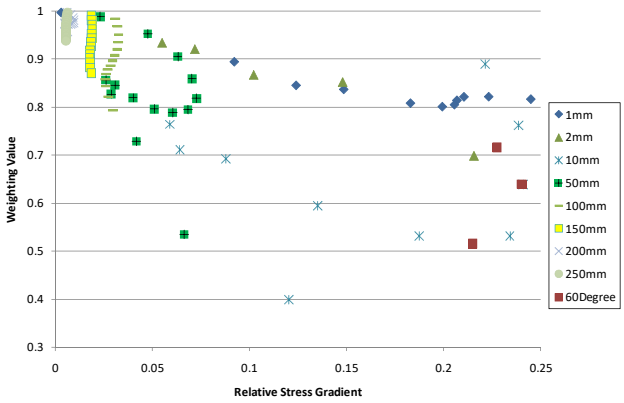


Fig. 20 Absolute Weighting Function Values for Notch

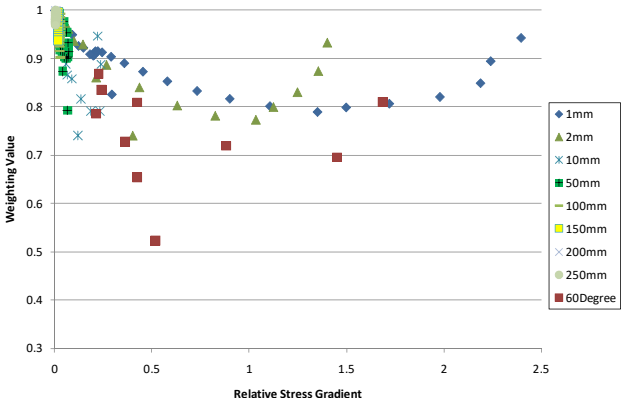


Fig. 21 Exponential Weighting Function for Notch Cases (0-2.5 Relative Stress Gradient)

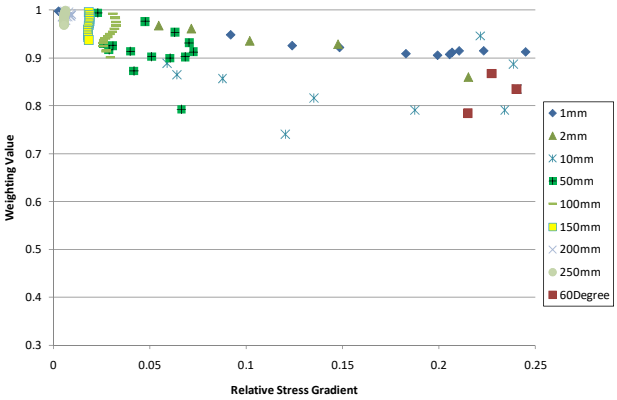


Fig. 22 Exponential Weighting Function Values for Notch Cases (0-0.25 Relative Stress Gradient)

## ACKNOWLEDGMENT

The author wishes to acknowledge Timothy Mckinley of Bradley University for his thesis work leading to this publication.

## REFERENCES

[1] G. Pluvinage and M. Gjonaj (eds), Notch Effects in Fatigue and Fracture, 1-22. Kluwer Academic Publishers, Netherlands, 2001.
[2] G. Qylafku, Z, Azari, M. Gjonaj, G. Pluvinage, On the Fatigue Failures and Life Prediction for Notched Specimens. Materials Science, Vol. 34, No. 5, 1998.
[3] Y. Weixing. Stress field intensity approach for predicting fatigue life. Int. J Fatigue 15 No 3 (1992), 243-245.
[4] Y. Weixing, Xia Kaiquan and Gu Yi. On the fatigue notch factor, $K_f$. Int. J. Fatigue Vol. 17, No. 4 (1995), 245-251.
[5] G. R. Irwin, Trans. ASME, J. Appl mech. 24, 361. (1957).
[6] Y. Murakami. Stress Intensity Factors Handbook. Soc. Materials Sci., Japan, Vol. 4, 2001.
[7] G. Glinka, Calculation of Inelastic Notch-Tip Strain-Stress Histories under Cyclic Loading, Engineering Fracture Mechanics Vol. 22, No. 5, 839-854. Pergamon Press, 1985.
[8] Y. Murakami: Metal Fatigue: Effects of Small defects and Nonmetallic Inclusions. Elsevier Science Ltd., Oxford, UK, 2002.
[9] Y. Murakami and M. Endo, Quantitative Evaluation of Fatigue Strength of Metals Containing Various Small Defects or Cracks. Engng Fract. Mech. 17, 1-15. 1983.
[10] Y. Murakami and M. Endo, Effects of Hardness and Crack Geometries on $\Delta K_{th}$ of Small Cracks Emanating from Small Defects. The Behavior of Short Fatigue Cracks. Mechanical Engineering Publication, London,

275-293. 1986.
[11] Y. Murakami and M. Endo, Prediction Equation for $\Delta K_{th}$ of Various Metals Containing Small Defects in Terms of the Vickers Hardness (HV) and Square Root of the Projected Area of Defects. Current Japanese Material Research, Vol. 8: Fracture Mechanics. Society of Materials Science, Japan, 105-124. 1991.
[12] H. Nisitani, Bull. JSME, 11, 14, 1968.
[13] H. Nisitani and Y. Murakami, Stress Intensity Factors of an Elliptical Crack or a Semi-Elliptical Crack Subject to Tension. Int. Journ. of Fracture, Vol. 10, No. 3 353-368. 1974.
[14] R. Perez et al, Interpolative Estimates of Stress Intensity Factors for Fatigue Crack Growth Predictions. Engineering Fracture Mechanics Vol. 24, No. 4, 629-633. 1986.
[15] Y. Lui and S. Manadevan, Fatigue Limit Prediction of Notched Components Using Short Crack Growth Theory and an Asymptotic Interpolation Method. Engineering Fracture Mechanics, 2008, doi:10.1016/j.engfracmech.2008.06.006
[16] G. Chell. Engng Fracture Mech. 7, 137. 1975.
[17] G. Chell. The Stress Intensity Factors for Part through Thickness Embedded and Surface Flaws Subject to a Stress Gradient. Engng Fracture Mech. Vol. 8, 331-340. 1976.
[18] ASME Nonmandatory Appendix A, Article A-3000, Method for $K_I$ Determination.
[19] J. Bloom. Determination of the Stress Intensity Factor for Gradient Stress Fields. Journal of Pressure Vessel Technology, Vol. 99, Issue 3, 477-484. 1977.
[20] H. Bueckner. A Novel Principal for the Computing of Stress Intensity Factors. Zeitschrift fur angewandte Mathematik und Mechanik 50, 529-545. 1997
[21] J. Rice. Some Remarks on Elastic Crack-Tip Stress Field. Int. J. Solids Structures, 8, 751-758. 1972.
[22] Y. Liu et al. Numerical Methods for Determination of Stress Intensity Factors of Singular Stress Field. Engineering Fracture mechanics. 75, 4793-4803. 2008.
[23] S. Ju and H. Chung. Accuracy and Limit of a Least-Squares Method to Calculate 3D Notch SIFs. International Journal of Fracture, 148, 169-183. 2007.
[24] J. Xu et al. Numerical Methods for the Determination of Multiple Stress Singularities and Related Stress Intensity Coefficients. Engineering Fracture Mechanics, 63, 775-790. 1999.
[25] D. Taylor, Theory of Critical Distances, Elsevier Ltd. 2007.
[26] D. Bellett et al, The fatigue behavior of three-dimensional stress concentrations. International Journal of Fatigue 27 (2005), 207-221.
[27] R. Adib, et al, Application of Volumetric Method to the Assessment of Damage Induced by Action of Foreign Objects on Gas Pipes. Strength of Materials, Vol. 38, No. 4, 409-416. 2006.
[28] H. Adib-Ramezani and J. Jeong. Advanced Volumetric Method for Fatigue Life Prediction Using Stress Gradient Effects at Notch Roots. Computational Materials Science 39, 649-663. 2007.
[29] H. Tada, P. Paris, and G. Irwin, The Stress Analysis of Cracks Handbook, 3rd edition, ASME, New York, NY, 2000.